Integration of Sub-6-GHz and mm-Wave Bands With a Large Frequency Ratio for Future 5G MIMO Applications

MUHAMMAD ZADA[ID][1]**, IZAZ ALI SHAH**[ID][1]**, AND HYOUNGSUK YOO**[ID][1,2]**, (Senior Member, IEEE)**
[1]Department of Electronic Engineering, Hanyang University, Seoul 04763, Republic of Korea
[2]Department of Biomedical Engineering, Hanyang University, Seoul 04763, Republic of Korea

Corresponding author: Hyoungsuk Yoo (hsyoo@hanyang.ac.kr)

ABSTRACT The integration of sub-6-GHz and millimeter-wave (mm-wave) bands has become an important issue for future fifth generation (5G) wireless communications owing to their large frequency ratios. This paper proposes a compact-size dual-function antenna operating at 3.5 GHz and the mm-wave band (28 GHz) for 5G mobile applications using a frequency reconfigurability technique. The proposed antenna comprises a microstrip patch linked with a meandered radiating structure through a radio frequency PIN diode to achieve frequency reconfigurability between the two bands. A significant size reduction up to 15.3 mm × 7.2 mm × 0.508 mm for the proposed antenna was achieved using a meandered line structure and truncated ground plane. To enhance the functionality, 8 × 8 multiple-input multiple-output (MIMO) with possible long- and short-edge antenna placement configurations were demonstrated. The system exhibited satisfactory MIMO characteristics with wide decoupling −10 dB bandwidths of 7.4% and 4.8% at the low- and high-frequency bands, respectively, without utilizing any external decoupling structure. The simulated results were validated using fabricated prototypes, and good agreement was observed. Additionally, a safety analysis based on the specific absorption rate and power density at the prescribed frequency bands was conducted using a realistic human model, and the results were found to be in accordance with the safety guidelines. Owing to the integration of sub-6-GHz and mm-wave bands in a single compact structure with a large frequency ratio and good MIMO performance, the proposed antenna system is suitable for future 5G mobile handheld devices.

INDEX TERMS Frequency reconfigurability, MIMO, mm-wave, PIN diodes, power density, smartphones, specific absorption rate, sub-6-GHz, truncated ground structure.

I. INTRODUCTION

Mobile communication is commonly used in daily life and is one of the most active areas of social development. Owing to the rapid growth of data and information, modern wireless networks need a high-speed data rate with low latency. Fifth generation (5G) for cellular and local area networks is foreseen to be a promising solution to overcome the limitations of current communication technologies [1]. The Federal Communications Commission has proposed the millimeter-wave (mm-wave) spectrum as the operating frequency for 5G communication, including 24, 28, 37–39, and 60 GHz [2]–[4].

The associate editor coordinating the review of this manuscript and approving it for publication was Hassan Tariq Chattha[ID].

However, the proposed spectrum involves challenges and shortcomings regarding propagation, which could also affect network deployment. Therefore, the prime 5G mid-band (3.4–3.6 GHz) has been assigned by the ITU WRC-15 and has already been deployed for the broadband cellular communication system; this band can offer wider area coverage with fewer propagation losses, while the mm-wave bands for short-range indoor links are still in developing stages [5]. The prime 5G band with upcoming mm-wave bands (e.g., 28 GHz) will be suitable for dense 5G small-cell networks in urban areas where additional capacity is vital. These frequency bands also suit macro-cells for wider area coverage. To support a large amount of traffic with a high data rate, the fastest 5G services require approximately 100-MHz

bandwidth in the 5G mid-band (3.5 GHz), and 1-GHz bandwidth at the mm-wave band (28 GHz). To meet these targets, several countries (including South Korea) have awarded bandwidths of 80 and 800 MHz per operator in the 3.5- and 28-GHz bands, respectively [6].

To cover the sub-6-GHz and mm-wave bands, antennas with multiband capability and a large frequency ratio are of great importance for future 5G applications [7]. Significant research efforts have been made to design antennas for sub-6-GHz 5G communication [8]–[16]; further, several compact-sized mm-wave antennas have been proposed [17]–[19]. Most reported studies used separate antennas for the corresponding frequency bands. However, space limitation in the handsets for several single-band antennas is a very challenging task. Therefore, the integration of the sub-6-GHz and mm-wave bands has attracted researchers' interest in this area. Future 5G technology demands compact-sized antennas with the capability of frequency reconfiguration to cover the allocated wireless frequency bands, e.g., sub-6-GHz and mm-wave bands. Reconfigurable antennas are advantageous over wideband and multiband antennas owing to their band notching capability to avoid interference [20].

Recently, several frequency-reconfigurable antennas for 5G applications have been proposed [21]–[27]. In [21], the author designed a pair of frequency-reconfigurable dipole antennas backed by an artificial magnetic conductor surface, covering the 3.3–3.6 GHz and 4.8–5.0 GHz bands for possible 5G applications. However, the overall size of the proposed structure was very large (72 mm × 72 mm × 3.5 mm) and was unable to achieve the 5G mm-wave bands. A microfluidic-based frequency-reconfigurable antenna covering the 5G band (3.5 GHz) was presented in [22], where piezoelectric pumps were used to realize wideband frequency tuning. The integration of the applied techniques in portable devices is significantly complex. Similarly, in [23], a differentially fed antenna with frequency-reconfigurable characteristics was developed for WLAN and sub-6-GHz 5G applications. The large size (100 mm × 100mm × 2.5 mm), two-layered structure, and the number of switches made the design inappropriate for smart handheld devices. In [24], the authors proposed a low-profile slotted T-shaped frequency-reconfigurable antenna intended for 5G wireless networks. The slots were designed with two pairs of switches to reconfigure the radiating structure at the desired frequencies of 26.5 and 40 GHz. The reconfigurable antenna designed in [25] exhibited four operating states (0.7, 2.4, 3.5, and 5.5 GHz) using varactor diodes. However, the antenna only covered the sub-6-GHz bands and had low gain values that were insufficient for satisfactory 5G communication services. The reconfigurable antennas presented in the literature are single-antenna elements with the corresponding limitations, and they are unable to cover both sub-6-GHz and mmm-wave bands. However, in many countries including the USA and South Korea, the prime 5G mid-band (3.5 GHz) and mm-wave band (28 GHz) have been assigned for future 5G communication.

The tremendous growth in 5G communication requires a system with high throughput capability and efficient spectrum utilization [28]. Moreover, new services and standards are continuously being added to wireless devices. It is challenging to design an antenna system that can support multiple wireless standards with the capability of high data rate and efficient spectrum utilization. The utilization of a multiple-input and multiple-output (MIMO) system with frequency-agile capability is the best candidate to address the aforementioned issues. Frequency-reconfigurable MIMO antenna systems combine the advantages of high throughput capability and several band coverages. To the best of the authors' knowledge regarding the MIMO antenna system with frequency-reconfigurable features, the relevant studies have not yet addressed both the 5G mid-band (3.5 GHz) and mm-wave band (28 GHz) owing to the large frequency ratio. Thus, a MIMO antenna system in the lower and higher bands of the 5G spectrum is required for handheld devices to cover the allocated bands by altering the switching state. Further, the majority of the previous studies did not consider user safety at 5G bands, e.g., by analyzing the specific absorption rate (SAR) and power density (PD).

In this paper, a compact dual-band frequency-reconfigurable antenna is proposed for future 5G handheld devices. A radio frequency (RF) PIN diode switch is used to provide two working states; thus, the proposed antenna can maximally cover 3.39–3.66 GHz (ON state) and 27.40–28.60 GHz (OFF state) for 5G applications. A significant size reduction and bandwidth enhancement were achieved using a meandered radiating patch and a truncated ground structure. Moreover, to enhance channel capacity and spectral efficiency for future 5G communication, 8 × 8 MIMO with possible short- and long-edge antenna placement configurations were formed. Owing to the meandered radiating structure and defected ground plane, satisfactory decoupling bandwidths were achieved for both configurations without utilizing external decoupling structures. Prototypes of the proposed proof-of-concept system were built, and the performance was validated through measurements. The measured results reasonably correlate with the simulations. For safety concerns, SAR and PD analyses were conducted at low and high frequencies, respectively. Both the SARs and PDs were found to comply with the prescribed safety limits of the Institute of Electrical and Electronics Engineering (IEEE) and the International Commission on Non-Ionizing Radiation Protection (ICNIRP). The proposed MIMO system offers the advantages of a simple structure, reasonable gain, high radiation efficiency, and frequency reconfiguration, making it well-suited for low- and high-frequency 5G applications, in contrast to the existing state-of-the-art MIMO antenna system.

II. METHODOLOGY
A. DESIGN OF 8 × 8 MIMO ANTENNA CONFIGURATIONS
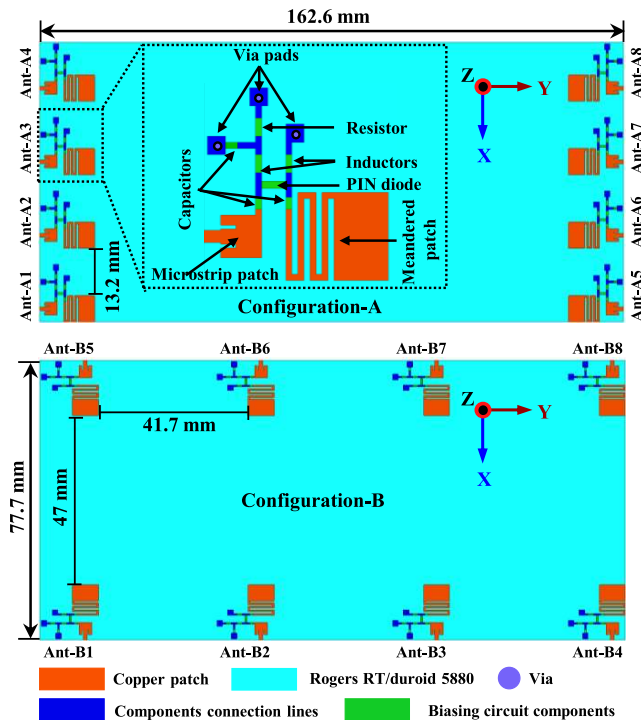The geometry of the proposed 8 × 8 MIMO antenna system with configurations A and B is illustrated in Fig. 1.

FIGURE 1. Geometry and dimensions of the proposed frequency-reconfigurable 8 × 8 MIMO antenna system with short and long-edge antenna configurations (Units: mm).

FIGURE 2. Detailed geometry and dimensions of the single antenna element (Units: mm): (a) Top view with PIN diode boundaries. (b) Rear view.

In configuration A, the eight-antenna elements (Ant-A1–Ant-A8) are symmetrically arranged along the two short edges of the substrate, while in configuration B, the antenna elements (Ant-B1–Ant-B8) are disposed along the long edges of the system substrate. To obtain the minimum isolation, 13.2 and 41.7 mm separations were set for the two closest antenna elements in configurations A and B, respectively. The designed eight-antenna elements are printed on the Rogers RT/duroid 5880 substrate with ε_r of 2.2, loss tangent (tanδ) of 0.0009, and thickness of 0.508 mm. The type and thickness of the substrate were selected to compensate for the losses in the mm-wave band and fabrication capabilities. The standard dimensions of 162.6 mm × 77.7 mm, equivalent to the Samsung Galaxy S10 5G were selected for the system substrate. The radiating patches with the corresponding switching technique and ground planes are printed on the front and back surfaces of the substrate, respectively. The antenna system design and optimization were conducted using the finite element method-based simulator ANSYS HFSS. Safety evaluations, such as SAR and PD analysis, were carried out using a realistic human body model in the finite difference time domain (FDTD)-based solvers Sim4Life^{TM} (Zurich MedTech AG, Switzerland). The head effects on the radiation patterns were evaluated using FDTD based Remcom.

B. DESIGN OF THE SINGLE-ANTENNA ELEMENT

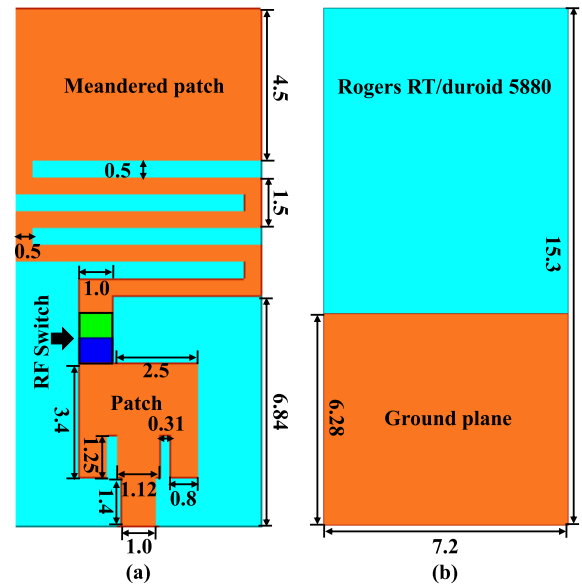The geometry of the proposed dual-band frequency-reconfigurable single-antenna element, including its detailed dimensions, is illustrated in Fig. 2. The antenna radiator comprises two parts: a rectangular patch and a meandered radiating structure connected through a PIN diode switch, as shown in Fig. 2(a). The proposed single-antenna element has a compact size of 15.3 mm × 7.2mm × 0.508 mm. A truncated ground structure, as shown in Fig. 2(b), is used to achieve miniaturization and wide bandwidth. The antenna is fed through a 50-Ω matched microstrip feed line with a width of 1 mm.

By utilizing the reconfigurability property, the microstrip antenna part is combined with the meandered part to form a single structure to be operated at a sub-6-GHz (3.5 GHz). The PIN diode is placed between the two parts to resonate the antenna at 3.5 and 28 GHz by altering the switching state. The DC blocking capacitors are placed between the two parts to block the entry of DC biasing voltage into the RF source. During the ON state of the PIN diode, the antenna operates at 3.5 GHz; whereas, in the OFF state, it operates in the mm-wave band at 28 GHz. The proposed eight-element frequency-reconfigurable MIMO antenna was fabricated in both configurations. The silicon PIN diode (BER90-22EL) from Infineon is used in the proposed design owing to its low insertion loss and fast switching time. In each configuration, eight PIN diodes are soldered, accompanied by biasing circuitries on the top surface of the substrate. The biasing voltage to the PIN diode is provided through the jumper wires. The equivalent circuits used in the simulations for the corresponding ON and OFF states are shown in Fig. 3. A very low resistance of 2.7 Ω and an inductance of 0.4 nH were considered for the PIN diode in the ON state. To obtain a good correlation between the measurements and simulation results, the PIN diode should provide the same

resistance and inductance in the measurements; thus, these values were considered based on the technical datasheet of BER90-22EL. Additionally, Fig. 3 provides details of the biasing circuitry used in the measurements, which includes RF chokes of 68 nH, DC biasing capacitors of 8.2 pF, and biasing voltage of 3.3 V (applied to the DC bias terminal). Further, in the simulation for the OFF state of the PIN diode, the capacitance and reverse resistance of each diode were assigned as 0.2 pF and 1.6 kΩ, respectively, according to the datasheet of BER90-22EL when biasing voltage of 0 V was applied.
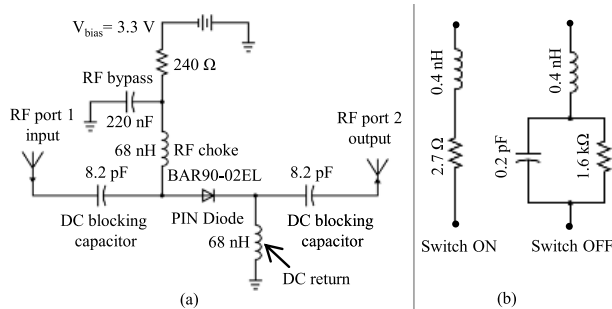

FIGURE 3. Equivalent circuits for the radio frequency PIN diode switch between ON and OFF states: (a) Biasing circuit of the proposed antenna used in the measurements. (b) Equivalent circuits used in the simulations for the corresponding ON and OFF states.

The surface current distributions of the proposed antenna at the corresponding frequencies are shown in Figs. 4(a) and (b). These intuitively describe the working principle of the antenna. In the ON state (Fig. 4(a)), the switch allows the current to flow from the microstrip patch part to the meandered structure that is responsible for resonating at 3.5 GHz. In the OFF state, the switch limits the radiating structure to only the microstrip patch part; thus, the current distribution is concentrated only on the microstrip patch, as shown in Fig. 4(b), resulting in resonance at 28 GHz.

III. PERFORMANCE ANALYSIS AND DISCUSSIONS

The simulated reflection coefficients of the antenna elements in configuration A and their corresponding isolations at 3.5 and 28 GHz are shown in Figs. 5(a) and (b), respectively. Meanwhile, Figs. 5(c) and (d) show the reflection coefficients and isolations for configuration B at the corresponding lower and higher frequency bands, respectively. As depicted in Fig. 5, in both configurations, the proposed MIMO antenna covers the targeted prime 5G 3.5 GHz band (3.45–3.55 GHz) when the switch is turned ON, while in the OFF state, the antenna operates at the mm-wave band 28 GHz with a satisfactory bandwidth of 1060 MHz. All the antenna elements in both configurations showed good impedance matching. The reflection coefficients of some antenna elements deviated slightly at 3.5 GHz in configuration A owing to their close placement; however, the achieved bandwidths were still sufficient to cover the targeted band.

The proposed MIMO antenna system was also evaluated for mutual coupling among various antenna elements in both
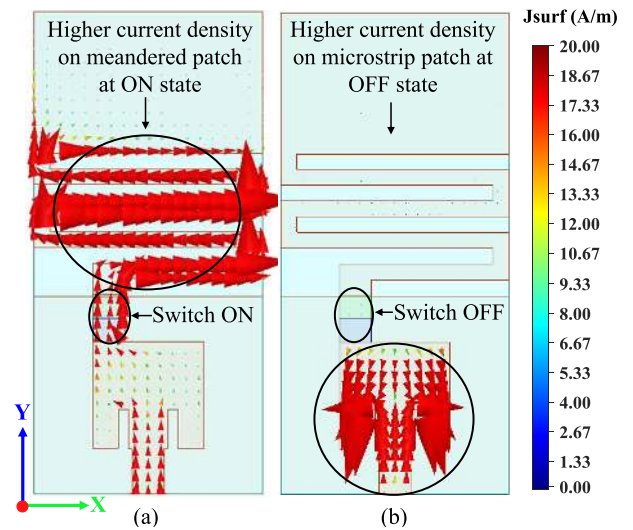

FIGURE 4. Current distributions on the radiating patch of a single antenna element: (a) ON state (3.5 GHz). (b) OFF state (28 GHz).

configurations. Because of the similar structure and symmetrical placement of the antenna elements in each configuration, only transmission coefficients S_{12}–S_{18} (port-1 with each port) and S_{23} (port-2 with port-3) were evaluated. Owing to the meandered radiating structure and defected ground plane (reduced ground effects), desirable isolation was achieved even at the lower frequency band across the operational bandwidth. As can be seen in Figs. 5(a) and (c), the isolation of 14 and 24.5 dB was achieved at the prime 5G band (3.5 GHz) between the closest antenna elements in configurations A and B, respectively. Satisfactory isolation of 33.7 and 36.4 dB were acquired between the nearest antenna elements at the mm-wave band (28 GHz) for configurations A and B, respectively. The considerably improved isolation at 28 GHz
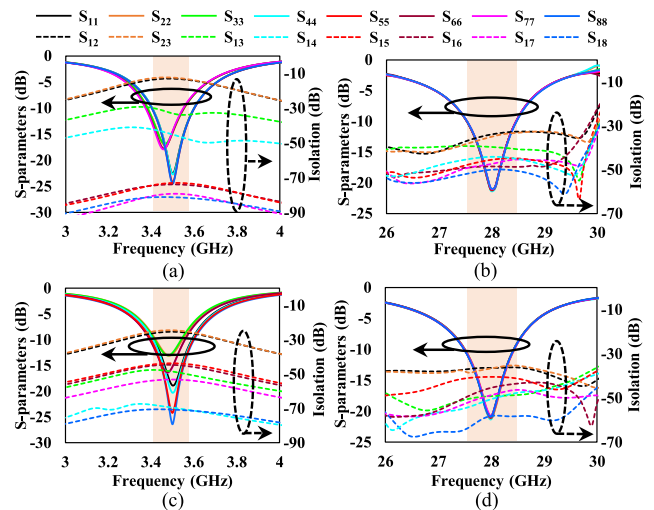

FIGURE 5. Simulated scattering parameters of the proposed 8 × 8 MIMO antenna system in various configurations: (a) ON state and (b) OFF state of PIN diode in configuration A. (c) ON state and (d) OFF state of PIN diode in configuration B.

was due to the very short wavelength in the mm-wave band. Although the isolation value between the closest antenna elements (Ant-A1 and -A2) at 3.5 GHz was comparatively small owing to the short distance between the antenna elements, the mutual coupling of the proposed MIMO antenna was still better than that of several 5G antennas at sub-6-GHz and mm-wave bands [9], [12], [15], [29].

To validate the performance of the proposed 5G MIMO antenna system, the envelop correlation coefficient (ECC) and diversity gain (DG) were evaluated. Acceptable performance can be achieved when ECC < 0.5 [28]. ECC can be calculated via several methods, e.g., using received signal envelopes, or by estimating the complex cross-correlation, using S-parameters or radiation patterns [30]. In this work, the simulated ECC was calculated from the radiation patterns of the antenna elements based on the following equations:

$$\rho_{ij} = \frac{|\iint_0^{4\pi} [\vec{F}_i(\theta, \phi) \times \vec{F}_j(\theta, \phi) d\Omega]|^2}{\iint_0^{4\pi} |\vec{F}_i(\theta, \phi)|^2 d\Omega \iint_0^{4\pi} |\vec{F}_j(\theta, \phi)|^2 d\Omega} \quad (1)$$

$$DG = 10\sqrt{1 - (ECC)^2} \quad (2)$$

where ρ_{ij} represents the ECC; $\vec{F}_i(\theta,\phi)$ and $\vec{F}_j(\theta,\phi)$ are the radiation patterns of the ith and j^{th} antenna elements, where i, j = 1, 2, 3, . . . , 8. Fig. 6 shows the simulated ECC performance of the proposed MIMO antenna system in both configurations for the corresponding switching states. The maximum ECC between the closest antenna elements was observed at 3.5 GHz with values of 0.11 and 0.02 for configuration A and B respectively, which were much lower than the acceptable ECC value of 0.5. Another important parameter for MIMO performance characterization is the DG, which quantifies the deterioration in the radiation performance of an antenna element using signal to noise ratio [31].
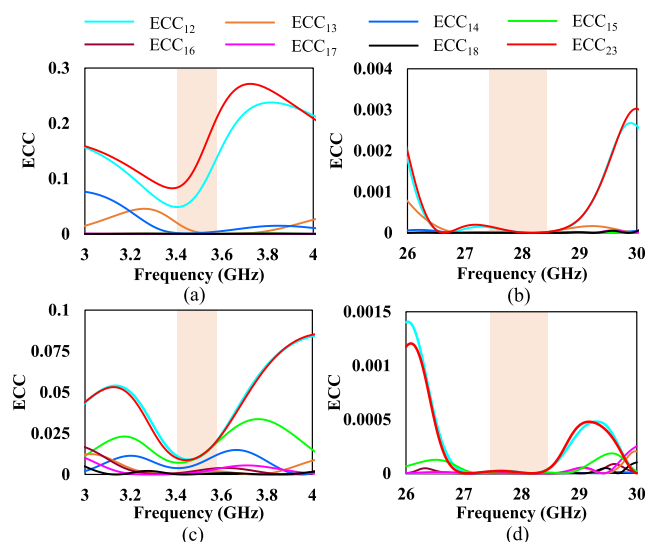
The corresponding DG values were calculated using equation 2 and are plotted in Fig. 7. As can be seen from Figs. 5 and 6, a good MIMO diversity performance was observed based on the computed ECC and DG values for all frequency bands in both configurations.
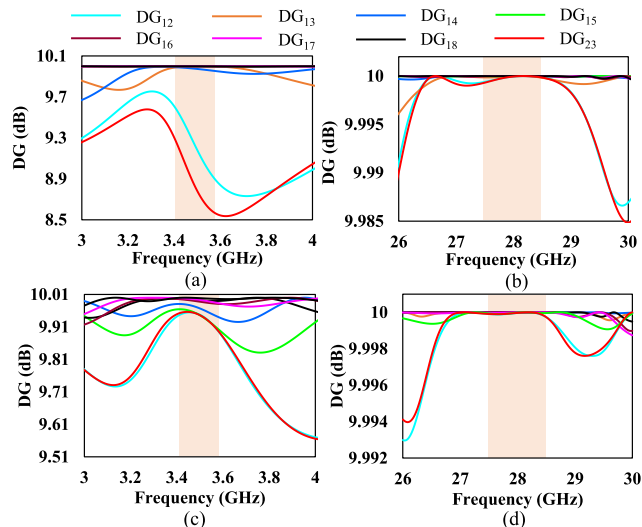
FIGURE 7. Simulated DG performance between antenna elements in various configurations: (a) ON state and (b) OFF state of PIN diode in configuration A. (c) ON state and (d) OFF state of PIN diode in configuration B.

Figs. 8(a) and (b) show the three-dimensional radiation patterns at both frequencies for configurations A and B. These patterns were evaluated in realistic human head and hand models in the FDTD-based simulator Remcom. As can be seen from Fig. 8, the proposed MIMO antenna elements in both configurations radiate outward. However, some of the antenna elements are in close contact with fingers, which slightly disturb the radiation behavior due to power absorption in hand tissues.

The important safety aspect regarding electromagnetic (EM) fields from wireless terminal devices is their coupling with the user's head and hand. International bodies such as the IEEE and ICNIRP have established safety guidelines to limit human exposure to EM waves. These guidelines provide basic restrictions in terms of (a) SAR to prevent tissue heating for frequencies less than 10 GHz and (b) PD to prevent tissue heating near the body surface for frequencies above 10 GHz [32]–[34]. Thus, to ensure user safety, the peak 10-g averaged SAR should not exceed 2 W/kg; whereas, the PD should be less than 10 W/m^2. A safety analysis of the proposed MIMO antenna in close proximity to the hand and head was conducted using the realistic human model Duke in Sim4Life. Figs. 9(a) and (b) show the distributions of the 10-g average SAR at the 3.5-GHz band for configurations A and B, respectively. An input power of 24 dBm was set for each antenna element because this has been used for the SAR calculation of long-term evolution smartphones; however, for mm-wave frequencies, the power standard has not yet been defined [29].
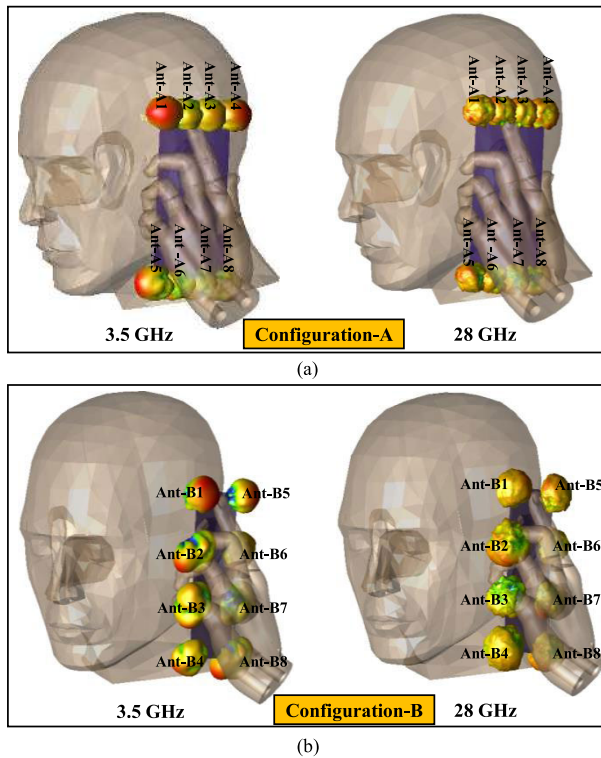
FIGURE 6. Simulated ECC performance between antenna elements in various configurations: (a) ON state and (b) OFF state of PIN diode in configuration A. (c) ON state and (d) OFF state of PIN diode in configuration B.

FIGURE 8. 3D radiation behavior of the proposed 8 × 8 MIMO antenna elements at both the operating bands: (a) Configuration A. (b) Configuration B.
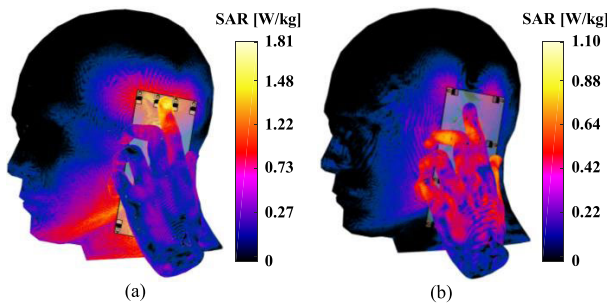

FIGURE 9. Peak 10-g average SAR distributions of the proposed 8 × 8 MIMO antenna system at 3.5 GHz: (a) Configuration A. (b) Configuration B.

FIGURE 10. PD distributions of the proposed 8 × 8 MIMO antenna system at 28 GHz: (a) Configuration A. (b) Configuration B.

FIGURE 11. PD field strength along a 15-mm line: (a) Configuration A. (b) Configuration B.

As expected, the maximum peak SAR was observed at the finger closest to the antenna element in each configuration, as shown in Fig. 9; however, it was in compliance with the safety limits in the ICNIRP guidelines. The peak 10-g average SAR values for each port in both configurations are summarized in Table 1.

To prevent tissue heating at higher frequencies (>10 GHz), PD is currently preferred because of the difficulty in determining a reasonable averaging volume for SAR estimation at very low penetration depth [35]. Considering a realistic scenario, the distance between the MIMO antenna system (ground surface) and the head surface was set to approximately 15 mm. The PD distributions for both configurations
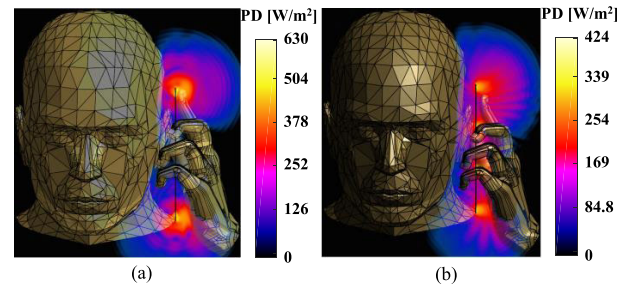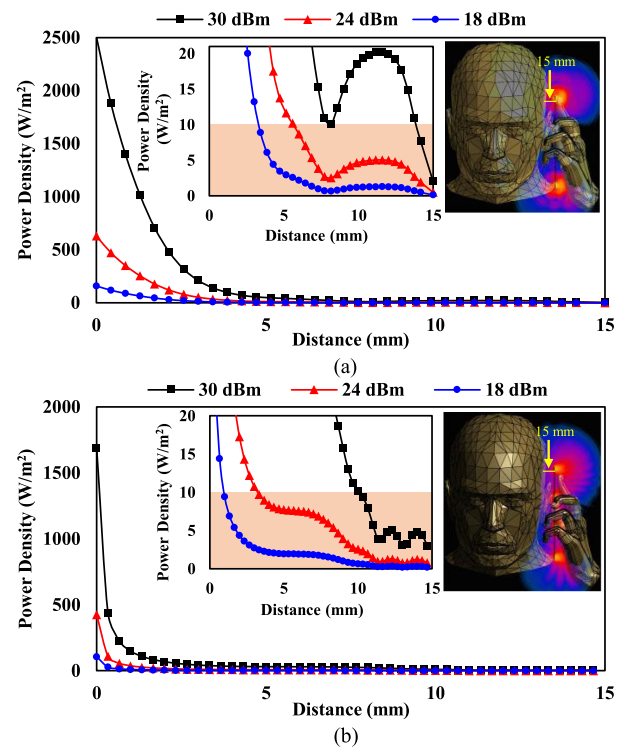
at 28 GHz are shown in Fig. 10. Moreover, Figs. 11(a) and (b) show the spatial PD strengths along the line (15 mm) for configurations A and B, respectively. The corresponding maximum peak PDs were 2500 and 2000 W/m^2 and decreased with the distance, as depicted in Figs. 11(a) and (b) (zoomed inset views). The PD exposure into the human head model was estimated for every port and is listed in Table 1. The maximum PD values in both configurations complied with the prescribed limit of 10 W/m^2 at the head surface for an input power of 24 dBm.

IV. MEASURED RESULTS

The 8 × 8 MIMO antenna prototypes in both configurations were fabricated and measured to validate the simulation results. End launch connectors (50 Ω) from the southwest microwave were used for measurement purposes.

TABLE 1. SAR and PD Values from Different Ports at 3.5 and 28 GHz.

	Frequency (GHz)	Safety Metrics	P1	P2	P3	P4	P5	P6	P7	P8
Configuration-A	3.5	SAR (W/kg)	0.78	1.66	1.81	0.70	0.76	0.78	0.77	0.80
	28	PD (W/m²)	0.81	1.69	1.97	0.97	0.69	0.75	0.79	0.85
Configuration-B	3.5	SAR (W/kg)	0.69	1.10	0.95	0.80	0.73	0.76	1.04	0.57
	28	PD (W/m²)	1.24	0.96	0.88	0.98	1.06	0.82	0.96	0.98

The fabricated MIMO antenna system with configurations A and B are shown in Figs. 12(a) and (b), respectively. The scattering parameters were measured using the E8364B Network Analyzer from Agilent Technology. The measured performances are discussed in the following subsections.
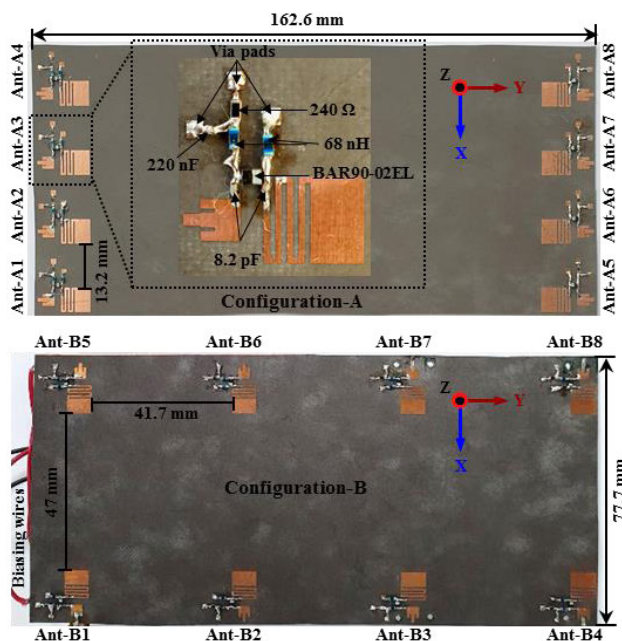
A. SCATTERING PARAMETERS

FIGURE 12. Fabricated prototypes of the proposed MIMO antenna system in both configurations with an enlarged view of a single antenna element with biasing circuitry.

The measured reflection coefficient and isolation curves for both configurations are shown in Figs. 13(a)-(d) at the corresponding low and high-frequency bands. Owing to the symmetric structure and placement of the antenna elements in each configuration, the reflection coefficient and isolation measurement results are shown only for the five ports. In general, the measured scattering performances of the proposed MIMO antenna were in good agreement with the simulation results. However, slight discrepancies were observed owing
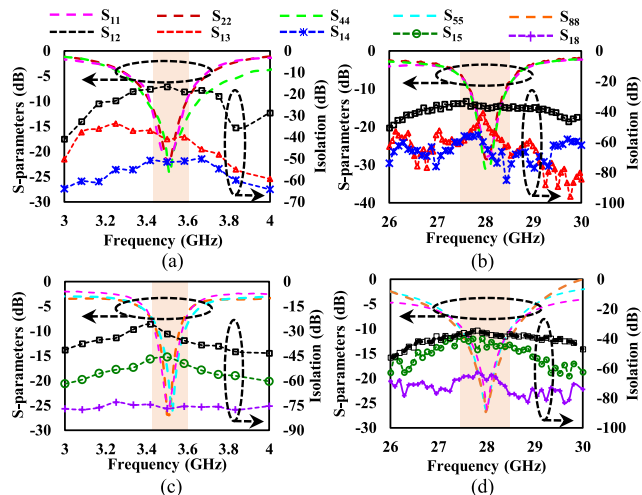

FIGURE 13. Measured scattering parameters of the proposed 8 × 8 MIMO antenna system in various configurations: (a) ON state and (b) OFF state of PIN diode in configuration A. (c) ON state and (d) OFF state of PIN diode in configuration B.

to fabrication tolerances and losses in the end launch connectors, resistors, and DC bias lines. As shown in Fig. 13, satisfactorily measured bandwidths for both configurations are achieved, which are sufficiently wide to support the desired 3.5- and 28-GHz bands. The measured bandwidths at 3.5 and 28 GHz for configuration A were 270 MHz (3.39–3.66 GHz) and 900 MHz (27.6–28.5 GHz), respectively; whereas, configuration B exhibited 140 MHz (3.45–3.59 GHz) and 1200 MHz (27.4–28.6 GHz) for the ON and OFF states, respectively. Fig. 13 also demonstrates the measured isolations between the antenna elements in both configurations at the corresponding frequencies. Minimum measured isolations of 16.4 and 36.4 dB were observed between the closest antenna elements Ant-A1 and Ant-A2 (configuration A) at 3.5 and 28 GHz, which is promising compared to the simulated isolation of 14 dB. The obtained measured isolations in both configurations across the targeted bandwidths are advantageous for attaining good diversity and multiplexing performances.

B. MEASURED ECC AND DG

As aforementioned, the ECC can be calculated from the far-field pattern data and S-parameters. Calculating the ECC from the measured radiation pattern involves a time-consuming integral calculation. To facilitate the process, the measured ECC values for the proposed MIMO antenna system were calculated based on the measured S-parameters using the following equation [36].

$$\rho_{ij} = \frac{|S_{ii}^* S_{ij} + S_{ji}^* S_{jj}|^2}{(1 - (|S_{ii}|^2 + |S_{ij}|^2))(1 - (|S_{jj}|^2 + |S_{ij}|^2))} \quad (3)$$

The measured ECCs among the five antenna elements in each configuration are shown in Figs. 14(a)–(d). A maximum ECC value of 0.02 was observed between the closest antenna element in configuration A, which was far below the
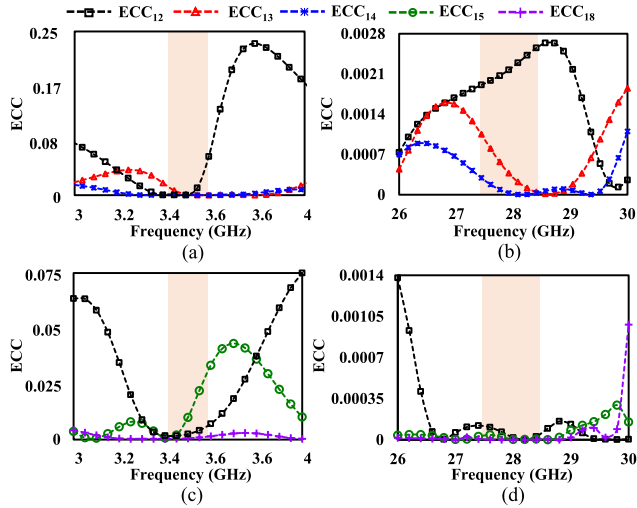
FIGURE 14. Calculated ECC from the measured results in various configurations: (a) ON state and (b) OFF state of PIN diode in configuration A. (c) ON state and (d) OFF state of PIN diode in configuration B.

acceptable criterion (ECC < 0.5). The measured ECC values based on the S-parameters were smaller than the simulated values because the proposed MIMO antenna system exhibited a very high efficiency (>90%) in both frequency bands. Based on the attained ECC values, the corresponding DG values were evaluated and are plotted in Fig. 15. The highest measured DG values of 9.97 and 9.99 dB were observed for configuration B at 3.5 and 28 GHz, respectively. The measured DG values correlate well with the simulated values and are sufficiently good for MIMO performance.
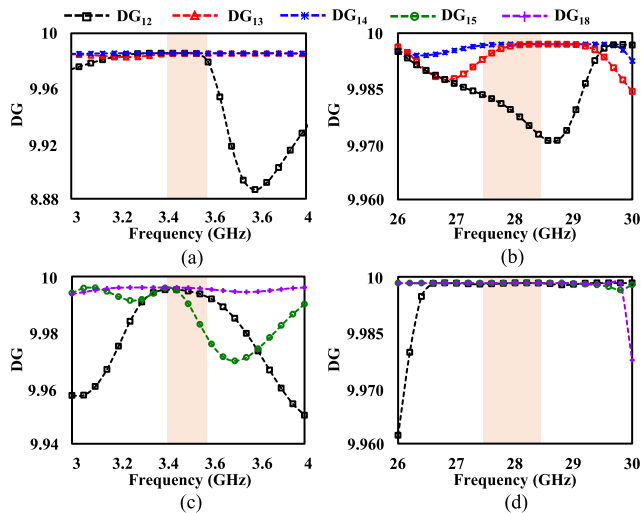

FIGURE 15. Calculated DG based on the measured ECC: (a) ON state and (b) OFF state of PIN diode in configuration A. (c) ON state and (d) OFF state of PIN diode in configuration B.

A comparison of the simulated and measured radiation patterns (co- and cross-polarization) for Ant 1 (other element ports terminated with 50-Ω matched loads) of both
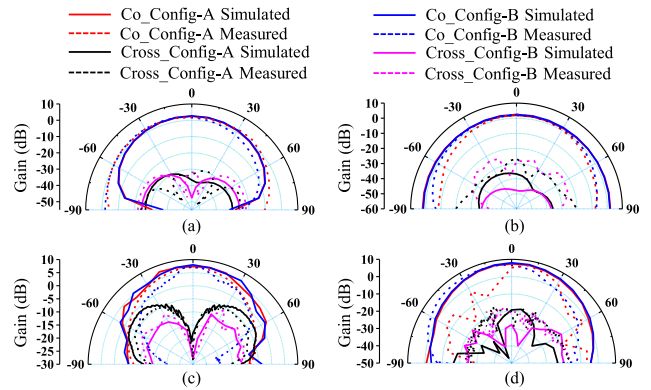

FIGURE 16. Simulated and measured co-and cross-radiation patterns for configurations A and B: Co- and cross-comparison in (a) azimuthal plane at 3.5 GHz, (b) elevation plane at 3.5 GHz, (c) azimuthal plane at 28 GHz, and (d) elevation plane at 28 GHz.

configurations are shown in Figs. 16(a)–(d). The radiation patterns of the other antenna elements in both configurations are omitted as they have similar patterns. Fig. 16(a) shows the measured and simulated radiation patterns in the azimuthal (E-plane) and elevation (H-plane) planes for co- and cross-polarization at 3.5 GHz. The maximum radiation occurred at $\theta = 0°$ in both configurations, while a difference of more than 30 dB between co- and cross-components was observed. A similar behavior was observed in the elevation plane in Fig. 16(b) for both cases. The co-polarization in the elevation plane is more than 30 dB over the cross-polarization, which shows the EMC feature of the proposed antenna. Figs. 16(c) and (d) show the 2D polar radiation pattern in the E- and H-planes for both co- and cross-polarization at 28 GHz, respectively. Directional radiation was observed in both planes with a difference of more than 15 dB between co- and cross-components. Additionally, in all cases, a reasonable correlation was noted between the simulated and measured results. A small distortion can be observed in the radiation patterns at the high-frequency band because of the current nulls, which increase with frequency. Moreover, these small discrepancies may be due to the losses in the end launch connectors and biasing circuity. The peak realized gain and total efficiency for configurations A and B at the
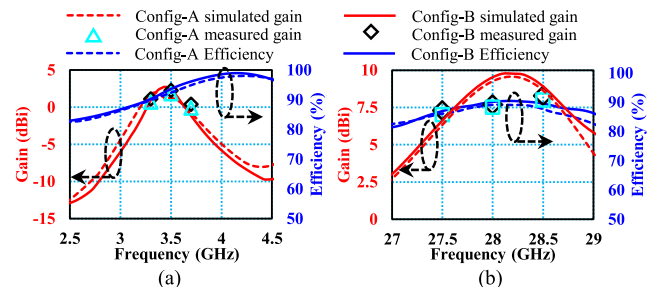

FIGURE 17. Efficiency and realized gain of the proposed 8 × 8 MIMO antenna system against the desired frequency bands in various configurations: (a) ON state (3.5 GHz). (b) OFF state (28 GHz).

TABLE 2. Proposed frequency reconfigurable MIMO antenna comparison with state-of-the-art 5G antennas.

Ref.	Year	Antenna size (mm³)	Frequency (GHz)	Bandwidth (%)	Gain (dBi)	Efficiency (%)	Safety study?	Sub-6 GHz 5G bands?	mm-Wave bands?	Frequency reconfigurability?	Frequency ratio	MIMO? sub-6 GHz	mm-wave
[12]	2017	18.6 × 18.8 × 1	2.6/ 3.5	3.84²/ 7.74²	3/--	50/62	No	Yes	No	No	1.35	Yes	N/A
[15]	2018	7 × 37 × 0.8	3.6/5.5	23¹/15¹	N/A	--/ 40	No	Yes	No	No	1.53	Yes	N/A
[16]	2019	45 × 40 × 0.508	2.4/ 5.5/ 28	15.8²/ 23.5²/ 11.3²	1.9/ 3.8/ 7.4	--/ -- /--	No	No	Yes	No	11.66	No	No
[17]	2020	43 × 33.9 × 0.254	3.5/ 28	20.7²/20.5²	7.07/ 11.31	N/A	No	Yes	Yes	No	8.0	Yes	N/A
[21]	2019	72 × 72 × 3.5	3.5/ 5.5	21.7²/ 25²	6.86/ 8.14	70/ 80	No	Yes	No	Yes	1.57	No	N/A
[22]	2016	90 × 45 × 3.5	2/ 2.6/ 3	--/ -- /--	2.7/ 3/ 3.1	92/ 89/ 87	No	No	No	Yes	1.50	No	N/A
[23]	2019	100 × 100 × 5.7	2.45/ 3.5	11.9²/ 6.6²	6.5/ 6.8	64.5/ 69.5	No	Yes	No	Yes	1.43	No	N/A
[25]	2019	25 × 15 × 0.2	0.7/ 2.4/ 3.5/ 5.5	33¹/ 47¹/ 11¹/ 12.7¹	1.7/ 1.3/ 2.1/ 2	60/ 63/ 65/ 6	No	Yes	No	Yes	6.11	No	N/A
This work	**2020**	**15.3 × 7.2 × 0.508**	**3.5/ 28**	**7.4²/ 4.7²**	**2.3/ 7.7**	**93.6/ 98.6**	**Yes**	**Yes**	**Yes**	**Yes**	**8.0**	**Yes**	**Yes**

¹ (-6 dB) impedance bandwidth
² (-10 dB) impedance bandwidth

corresponding lower and higher frequency bands are shown in Figs. 17(a) and (b), respectively. The results are shown for Ant-A1 and -B1 only owing to the symmetrical placements of antenna elements in each configuration. In the ON state (3.5 GHz), the simulated and measured peak realized gain values for Ant-A1 were 1.88 and 1.76 dBi, while for Ant-B1, the corresponding values were 2.39 and 2.23 dBi, respectively. In the OFF state (28 GHz), the measured peak realized gain values for Ant-A1 and -B1 were 7.5 and 7.7 dBi, respectively. The total simulated radiation efficiencies for configurations A and B at 3.5 GHz were 92.39% and 93.66%, while at the 28 GHz band, the corresponding values were 97.14% and 98.6%, respectively. Thus, the simulated and measured results exhibit reasonable agreement. The small difference is due to the loss from the PIN diode switch, SMA connector, and coaxial line in the measurements.

C. COMPARISON WITH PRIOR WORKS

The proposed reconfigurable MIMO antenna system is compared based on some key parameters with recently published works in Table 2. It is apparent that by combining the total volume required for sub-GHz and 5G (mm-wave) antenna footprints, [16], [17] require a large antenna profile making them less suitable for handheld devices. Moreover, the frequency-reconfigurable antennas reported in [21]–[23], [25] are single-antenna elements with considerably large sizes, covering only sub-6-GHz 5G bands. Because of the limited space in handheld devices, reconfigurable antennas with large footprints are not suitable for MIMO smartphone applications. In this study, the proposed design successfully realizes the integration of sub-GHz and mm-wave bands for the first time in one compact structure

with a size of only 15.3 mm × 7.2 mm × 0.508 mm using the frequency reconfigurability technique. The proposed antenna system exhibits satisfactory gain and efficiency values with a considerably smaller size compared to existing antenna systems. Moreover, the safety aspects of the reported designs were not considered in previous studies.

V. CONCLUSION

In this paper, the integration of sub-6-GHz (3.5 GHz) and mm-wave (28 GHz) bands using a frequency reconfigurability technique was discussed for future 5G MIMO smartphone applications. The proposed antenna comprises a microstrip patch linked with a meandered line structure through a PIN diode to achieve reconfigurability between the two frequency bands by altering the switching state. The compact size for the single antenna element was achieved using a meandered line structure and truncated ground plane. The MIMO performance of the proposed concept was demonstrated for short- and long-edge antenna placement configurations. The system exhibited satisfactory MIMO performance across the entire bandwidth in both configurations. Moreover, a safety study was conducted out in accordance with the IEEE and ICNIRP safety guidelines. Based on the enhanced diversity and multiplexing performance, the proposed configurations fulfilled the requirements of the MIMO antenna system at sub-6-GHz and mm-wave bands; therefore, they are promising candidates for future 5G wireless applications.

REFERENCES
[1] M. Ikram, E. A. Abbas, N. Nguyen-Trong, K. H. Sayidmarie, and A. Abbosh, "Integrated frequency-reconfigurable slot antenna and connected slot antenna array for 4G and 5G mobile handsets," *IEEE Trans. Antennas Propag.*, vol. 67, no. 12, pp. 7225–7233, Dec. 2019.

[2] S. Li and C. Chris Mi, "Wireless power transfer for electric vehicle applications," *IEEE J. Emerg. Sel. Topics Power Electron.*, vol. 3, no. 1, pp. 4–17, Mar. 2015.

[3] W. Hong, K.-H. Baek, and S. Ko, "Millimeter-wave 5G antennas for smartphones: Overview and experimental demonstration," *IEEE Trans. Antennas Propag.*, vol. 65, no. 12, pp. 6250–6261, Dec. 2017.

[4] J. Yang, Y. Shen, L. Wang, H. Meng, W. Dou, and S. Hu, "2-D scannable 40-GHz folded reflectarray fed by SIW slot antenna in single-layered PCB," *IEEE Trans. Microw. Theory Techn.*, vol. 66, no. 6, pp. 3129–3135, Jun. 2018.

[5] P. Liu, X.-W. Zhu, Y. Zhang, X. Wang, C. Yang, and Z. H. Jiang, "Patch antenna loaded with paired shorting pins and H-Shaped slot for 28/38 GHz dual-band MIMO applications," *IEEE Access*, vol. 8, pp. 23705–23712, Jan. 2020.

[6] GSM Association, "5G spectrum-public policy position," GSM Assoc., London, U.K., Tech. Rep., Nov. 2016.

[7] J. F. Zhang, Y. J. Cheng, Y. R. Ding, and C. X. Bai, "A dual-band shared-aperture antenna with large frequency ratio, high aperture reuse efficiency, and high channel isolation," *IEEE Trans. Antennas Propag.*, vol. 67, no. 2, pp. 853–860, Feb. 2019.

[8] Z. Qin, W. Geyi, M. Zhang, and J. Wang, "Printed eight-element MIMO system for compact and thin 5G mobile handset," *Electron. Lett.*, vol. 52, no. 6, pp. 416–418, Mar. 2016.

[9] Y. Li, C.-Y.-D. Sim, Y. Luo, and G. Yang, "High-isolation 3.5 GHz eight-antenna MIMO array using balanced open-slot antenna element for 5G smartphones," *IEEE Trans. Antennas Propag.*, vol. 67, no. 6, pp. 3820–3830, Jun. 2019.

[10] Y.-L. Ban, C. Li, C.-Y.-D. Sim, G. Wu, and K.-L. Wong, "4G/5G multiple antennas for future multi-mode smartphone applications," *IEEE Access*, vol. 4, pp. 2981–2988, Jun. 2016.

[11] H. Piao, Y. Jin, and L. Qu, "A compact and straightforward self-decoupled MIMO antenna system for 5G applications," *IEEE Access*, vol. 8, pp. 129236–129245, Jul. 2020.

[12] M. Li, Z. Xu, Y. Ban, C. Sim, and Z. Yu, "Eight-port orthogonally dual-polarised MIMO antennas using loop structures for 5G smartphone," *IET Microw., Antennas Propag.*, vol. 11, no. 12, pp. 1810–1816, Sep. 2017.

[13] M.-Y. Li, Y.-L. Ban, Z.-Q. Xu, G. Wu, C.-Y.-D. Sim, K. Kang, and Z.-F. Yu, "Eight-port orthogonally dual-polarized antenna array for 5G smartphone applications," *IEEE Trans. Antennas Propag.*, vol. 64, no. 9, pp. 3820–3830, Sep. 2016.

[14] M. Ikram, N. Nguyen-Trong, and A. M. Abbosh, "Common-aperture sub-6 GHz and millimeter-wave 5G antenna system," *IEEE Access*, vol. 8, pp. 199415–199423, Oct. 2020.

[15] Y. Li, C.-Y.-D. Sim, Y. Luo, and G. Yang, "12-port 5G massive MIMO antenna array in sub-6GHz mobile handset for LTE bands 42/43/46 applications," *IEEE Access*, vol. 6, pp. 344–354, Oct. 2018.

[16] M. E. Yassin, H. A. Mohamed, E. A. F. Abdallah, and H. S. El-Hennawy, "Single-fed 4G/5G multiband 2.4/5.5/28 GHz antenna," *IET Microw., Antennas Propag.*, vol. 13, no. 3, pp. 286–290, Feb. 2019.

[17] J. Lan, Z. Yu, J. Zhou, and W. Hong, "An aperture-sharing array for (3.5, 28) GHz terminals with steerable beam in millimeter-wave band," *IEEE Trans. Antennas Propag.*, vol. 68, no. 5, pp. 4114–4119, May 2020.

[18] M. Khalily, R. Tafazolli, P. Xiao, and A. A. Kishk, "Broadband mm-wave microstrip array antenna with improved radiation characteristics for different 5G applications," *IEEE Trans. Antennas Propag.*, vol. 66, no. 9, pp. 4641–4647, Sep. 2018.

[19] Y. Zhang, J.-Y. Deng, M.-J. Li, D. Sun, and L.-X. Guo, "A MIMO dielectric resonator antenna with improved isolation for 5G mm-wave applications," *IEEE Antennas Wireless Propag. Lett.*, vol. 18, no. 4, pp. 747–751, Apr. 2019.

[20] S. F. Jilani, S. M. Abbas, K. P. Esselle, and A. Alomainy, "Millimeter-wave frequency reconfigurable T-shaped antenna for 5G networks," in *Proc. IEEE 11th Int. Conf. Wireless Mobile Comput., Netw. Commun.*, Oct. 2015, pp. 100–102.

[21] Z. Nie, H. Zhai, L. Liu, J. Li, D. Hu, and J. Shi, "A dual-polarized frequency-reconfigurable low-profile antenna with harmonic suppression for 5G application," *IEEE Antennas Wireless Propag. Lett.*, vol. 18, no. 6, pp. 1228–1232, Jun. 2019.

[22] A. Dey and G. Mumcu, "Microfluidically controlled frequency-tunable monopole antenna for high-power applications," *IEEE Antennas Wireless Propag. Lett.*, vol. 15, pp. 226–229, Jun. 2016.

[23] G. Jin, C. Deng, J. Yang, Y. Xu, and S. Liao, "A new differentially-fed frequency reconfigurable antenna for WLAN and sub-6GHz 5G applications," *IEEE Access*, vol. 7, pp. 56539–56546, Feb. 2019.

[24] S. F. Jilani, A. Rahimian, Y. Alfadhl, and A. Alomainy, "Low-profile flexible frequency-reconfigurable millimetre-wave antenna for 5G applications," *Flexible Printed Electron.*, vol. 3, no. 3, Aug. 2018, Art. no. 035003.

[25] L. Sun, H. Feng, Y. Li, and Z. Zhang, "Compact 5G MIMO mobile phone antennas with tightly arranged orthogonal-mode pairs," *IEEE Trans. Antennas Propag.*, vol. 66, no. 11, pp. 6364–6369, Nov. 2018.

[26] W. A. Awan, N. Hussain, S. A. Naqvi, A. Iqbal, R. Striker, D. Mitra, and B. D. Braaten, "A miniaturized wideband and multi-band on-demand reconfigurable antenna for compact and portable devices," *AEU-Int. J. Electron. Commun.*, vol. 122, Jul. 2020, Art. no. 153266. [Online]. Available: http://www.sciencedirect.com/science/article/pii/S1434841120305628

[27] N. Hussain, W. A. Awan, S. I. Naqvi, A. Ghaffar, A. Zaidi, S. A. Naqvi, A. Iftikhar, and X. J. Li, "A compact flexible frequency reconfigurable antenna for heterogeneous applications," *IEEE Access*, vol. 8, pp. 173298–173307, 2020.

[28] W. C. Mok, S. H. Wong, K. M. Luk, and K. F. Lee, "Single-layer single-patch dual-band and triple-band patch antennas," *IEEE Trans. Antennas Propag.*, vol. 61, no. 8, pp. 4341–4344, Aug. 2013.

[29] J. Bang and J. Choi, "A SAR reduced mm-wave beam-steerable array antenna with dual-mode operation for fully metal-covered 5G cellular handsets," *IEEE Antennas Wireless Propag. Lett.*, vol. 17, no. 6, pp. 1118–1122, Jun. 2018.

[30] S. Soltani, P. Lotfi, and R. D. Murch, "A port and frequency reconfigurable MIMO slot antenna for WLAN applications," *IEEE Trans. Antennas Propag.*, vol. 64, no. 4, pp. 1209–1217, Apr. 2016.

[31] A. Iqbal, A. Basir, A. Smida, N. K. Mallat, I. Elfergani, J. Rodriguez, and S. Kim, "Electromagnetic bandgap backed millimeter-wave MIMO antenna for wearable applications," *IEEE Access*, vol. 7, pp. 111135–111144, Aug. 2019.

[32] International Commission on Non-Ionizing Radiation Protection, "Guidelines for limiting exposure to time-varying electric and magnetic fields (1 Hz to 100 kHz)," *Health Phys.*, vol. 99, no. 6, pp. 818–836, 2010.

[33] I. Lagroye, "Gaps in Knowledge Relevant to the 'Guidelines for limiting exposure to time-varying electric and magnetic fields (1 Hz–100 kHz)," *Health Phys.*, vol. 118, no. 5, pp. 533–542, 2020. [Online]. Available: https://hal.archives-ouvertes.fr/hal-02903218

[34] W. H. Bailey, R. Bodemann, J. Bushberg, C. K. Chou, R. Cleveland, A. Faraone, K. R. Foster, K. E. Gettman, K. Graf, T. Harrington, and A. Hirata, "Synopsis of IEEE Std C95. 1-2019 'IEEE standard for safety levels with respect to human exposure to electric, magnetic, and electromagnetic fields, 0 Hz to 300 GHz," *IEEE Access*, vol. 7, pp. 171346–171356, Nov. 2019.

[35] T. Wu, T. S. Rappaport, and C. M. Collins, "Safe for generations to come: Considerations of safety for millimeter waves in wireless communications," *IEEE Microw. Mag.*, vol. 16, no. 2, pp. 65–84, Mar. 2015.

[36] Q. Rao and K. Wilson, "Design, modeling, and evaluation of a multi-band MIMO/diversity antenna system for small wireless mobile terminals," *IEEE Trans. Compon., Packag., Manuf. Technol.*, vol. 1, no. 3, pp. 410–419, Mar. 2011.

MUHAMMAD ZADA received the B.Sc. degree in telecommunication engineering from the University of Engineering and Technology, Peshawar, Pakistan, in 2015. He is currently pursuing the M.S./Ph.D. degrees in electronic engineering with Hanyang University, Seoul, South Korea.

He has published over 14 articles in high-quality journals and conferences proceedings in the field of telecommunications and biomedical engineering. He is serving as a Reviewer for the IEEE TRANSACTIONS, RFCAD, and Elsevier journals. His current research interests include implantable antennas and devices, intra-oral tongue drive systems, wireless power transfer, millimeter-wave antennas, wearable sensors and antennas, MRI and RF coils, microwave breast cancer detection, frequency-selective surfaces, and EBGs. He was awarded the Best Student Paper Competition 2018 from the Korean Institute of Electromagnetic Engineering and Science (KIEES).

IZAZ ALI SHAH received the B.Sc. degree in telecommunication engineering from the University of Engineering and Technology, Peshawar, Pakistan, in 2016. He is currently pursuing the M.S./Ph.D. degrees in electronic engineering with Hanyang University, Seoul, South Korea. He has coauthored seven journal articles and two conference papers. His current research interests include implantable antennas and devices, wireless power transfer to electric vehicles and implantable devices, MRI and RF coils, frequency selective surfaces, and EBGs.

Mr. Shah received fully funded scholarship awarded from the Prime Minister's National ICT Research and Development fund throughout the bachelor's degree program. He was awarded for the Best Student Paper Competition from the Korean Institute of Electromagnetic Engineering (KIEES), in 2018 and 2020. He is also serving as a Reviewer for the IEEE TRANSACTIONS and Elsevier Journals.

HYOUNGSUK YOO (Senior Member, IEEE) received the B.Sc. degree in electrical engineering from Kyungpook National University, Daegu, South Korea, in 2003, and the M.Sc. and Ph.D. degrees in electrical engineering from the University of Minnesota, Minneapolis, MN, USA, in 2006 and 2009, respectively.

In 2009, he joined the Center for Magnetic Resonance Research, University of Minnesota, as a Postdoctoral Associate. In 2010, he joined the Cardiac Rhythm Disease Management, Medtronic, MN, USA, as a Senior EM/MRI Scientist. From 2011 to 2018, he was an Associate Professor with the Department of Biomedical Engineering, School of Electrical Engineering, University of Ulsan, Ulsan, South Korea. Since 2018, he has been an Associate Professor with the Department of Biomedical Engineering and the Department of Electronics Engineering, Hanyang University, Seoul, South Korea. He has been the CEO of E2MR, a startup company, since 2017. His current research interests include electromagnetic theory, numerical methods in electromagnetics, metamaterials, antennas, implantable devices, and magnetic resonance imaging in high-magnetic field systems.

Dr. Yoo was awarded Third Prize for the Best Student Paper from the 2010 IEEE Microwave Theory and Techniques Society International Microwave Symposium.

• • •